

Vortex Pair Annihilation in Two-Dimensional Superfluid Turbulence

Woo Jin Kwon, Geol Moon, Jae-yoon Choi, Sang Won Seo, and Yong-il Shin*
*Center for Subwavelength Optics and Department of Physics and Astronomy,
 Seoul National University, Seoul 151-747, Korea*

We investigate thermal relaxation of two-dimensional superfluid turbulence in a highly oblate Bose-Einstein condensate. We identify annihilation of vortex-antivortex pairs by directly observing coalesced vortex cores with a crescent shape and their disappearing as being filled with atoms. The vortex number of the condensate exhibits nonexponential decay behavior due to the vortex pair annihilation process. We measure the two-body decay rate of the vortex number for various sample conditions and find that the local decay rate is proportional to T^2/μ , where T is the temperature and μ is the chemical potential.

PACS numbers: 67.85.De, 03.75.Lm, 67.25.dk

In a two-dimensional (2D) superfluid, quantized vortices are topological, point-like objects and they can be created and also annihilated as a pair of vortices of opposite circulation. Vortex-antivortex pairs play essential roles in 2D superfluid phenomena such as the Berezinskii-Kosterlitz-Thouless transition [1, 2], phase transition dynamics [3], and superfluid turbulence [4, 5]. Recently, controlled experimental studies of vortex dipole dynamics have been enabled in atomic Bose-Einstein condensate (BEC) systems [6, 7] and thermal activation of vortex pairs has been observed in quasi-2D Bose gases [8, 9]. However, the annihilation of a vortex-antivortex pair has not been clearly observed yet. In this Letter we present the first experimental study on the vortex pair annihilation in an atomic BEC.

Vortex pair annihilation is of particular importance in 2D superfluid turbulence. In 2D turbulence of a classical hydrodynamic fluid, the kinetic energy of the system flows toward large length scales due to the conservation of enstrophy which is integral of squared vorticity [10]. This is known as the inverse energy cascade and manifests itself in generating large-scale flow structures from small-scale forcing. This phenomenon is qualitatively different from three-dimensional (3D) turbulence where energy is typically dissipated into small length scales. An interesting question is whether the inverse cascade can occur in an atomic BEC. Since the enstrophy is not conserved in a compressible 2D superfluid due to the vortex-antivortex annihilation, there has been a theoretical controversy on this issue [11–16]. Recently, Neely *et al.* [17] reported an experimental and numerical study to demonstrate that there are conditions for which 2D turbulence in a BEC can dissipatively evolve into large-scale flow.

Here we investigate thermal relaxation of turbulent superflow in a highly oblate BEC. First, we identify the vortex-antivortex annihilation in the turbulent superflow by observing crescent-shaped, coalesced vortex cores which are partially filled with atoms. Secondly, we measure the temporal evolution of the vortex number in the relaxation process and observe nonexponential decay behavior, which we attribute to the vortex pair annihilation process being vortex density dependent.

In our experiment, the local two-body decay rate of the vortex number is found to be proportional to T^2/μ , where T is the temperature and μ is the chemical potential. This result provides valuable quantitative information on the vortex pair annihilation and thermal dissipation in 2D quantum turbulence.

We prepare a highly oblate BEC of ^{23}Na atoms in the $|F = 1, m_F = -1\rangle$ state in a harmonic trap, where the axial and radial confinements are provided by optical and magnetic trapping potentials, respectively. The magnetic potential is generated from an axially symmetric, magnetic quadrupole field [9]. The trapping frequencies are $\omega_{r,z} = 2\pi \times (15, 350)$ Hz. For a condensate of $N_0 = 1.8 \times 10^6$ atoms, the chemical potential is $\mu \approx k_B \times 60$ nK [18] and the radial Thomas-Fermi (TF) radius is $R = \sqrt{2\mu/m\omega_r^2} \approx 70 \mu\text{m}$, where m is the atomic mass. Because of the large aspect ratio of the condensate, $\omega_z/\omega_r > 20$, the vortex line excitations are highly suppressed [19] and the vortex dynamics in our system is expected to be two-dimensional. Note that $\mu > 3\hbar\omega_z$ and the condensate is thermodynamically 3D.

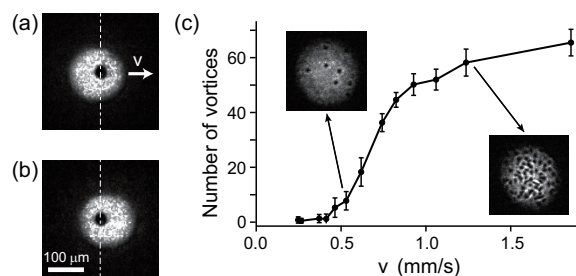


FIG. 1: Generation of turbulent flow in a BEC. A repulsive laser beam penetrates through the condensate and sweeps its center region by horizontally translating the trapped condensate by $37 \mu\text{m}$. In situ images of the condensate (a) before and (b) after the translation. (c) Number of the vortices in the perturbed condensate as a function of the translation speed v . The speed of sound is estimated to be $c \approx 4.6$ mm/s at the center of the condensate.

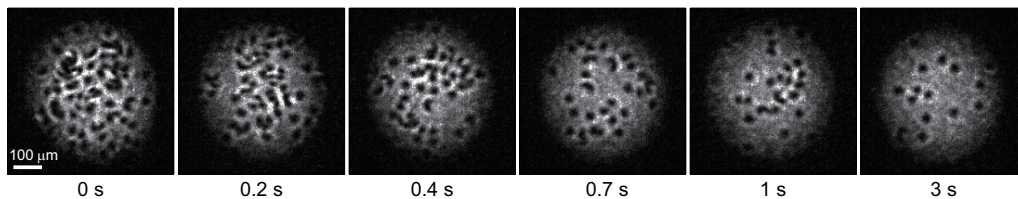


FIG. 2: Relaxation of turbulent superflow in a highly oblate BEC. (a) Examples of images for various relaxation times, where the atom number of the condensate $N_0 \approx 1.8 \times 10^6$ and the condensate fraction $\eta \approx 0.8$.

To generate turbulent flow in the condensate, we employ a repulsive Gaussian laser beam as a stirring obstacle [6]. Having the laser beam axially penetrating through the condensate, we horizontally translate the condensate by moving the magnetic trap center by $37 \mu\text{m}$ for 30 ms (Fig. 1), and adiabatically turn off the laser beam for 0.4 s. Here the laser beam, fixed in the lab frame, sweeps the center region of the condensate. The $1/e^2$ beam width is $15 \mu\text{m}$ and the barrier height is about 15μ . The translation speed corresponds to $\sim 0.3c$, where $c = \sqrt{\mu/m}$ is the speed of sound. We detect vortices in the turbulent flow by taking an absorption image after 24 ms time-of-flight [20]. With this procedure, we could generate over 60 vortices in our coldest sample without noticeable shape oscillations of the condensate [21]. The critical velocity for the vortex nucleation was measured to be $\approx 0.1c$ [Fig. 1(c)], which is consistent with the previous measurements [6, 22].

Figure 2 displays images of condensates with turbulent flow after various relaxation times. The condensates show disordered vortex distributions. At the early stage of the relaxation, some features seem to be suggestive of vortex clustering but we observed no evidence in the spatial analysis of the vortex distributions using Ripley's K -function [23]. The turbulent condensate eventually relaxes into a stationary ground state as the vortex number N_v decreases. In a condensate of finite spatial extent, there are only two ways for a quantum vortex to disappear: drifting out of the condensate boundary or being

annihilated inside the condensate as a vortex-antivortex pair. Both processes are driven by thermal dissipation which arises from the collisional exchange of atoms between the condensate and the thermal cloud [24].

The vortex pair annihilation occurs when the size of the vortex dipole becomes smaller than a certain threshold value, converting the energy into sound waves. It was numerically shown that coalescence of the vortex cores is followed by formation of a dark or gray soliton of a crescent shape, which eventually evolves into a shock wave [4, 25]. Indeed, we observe crescent-shaped density-depleted regions in the turbulent condensate (Fig. 3). These are coalesced vortex cores of opposite circulation and the bending structure can be accounted for by the linear momentum of the vortex dipole which is perpendicular to the vortex dipole direction. Furthermore, some of the coalesced vortex cores appear with significantly reduced visibility [Fig. 3(c)], indicating that they are disappearing by being filled up with atoms. This is clear evidence on the vortex-antivortex annihilation.

The vortex number N_v of the condensate is observed to show nonexponential decay behavior in the relaxation process [Fig. 4(a)]. This is expected from the fact that the vortex pair annihilation is a vortex density dependent process. At high vortex density n_v , a 2D turbulent superfluid can be considered as a gas of vortex-antivortex pairs [26, 27]. For a vortex pair of size d , the collisional cross section $\sigma \sim d$ and the linear velocity $v \sim \hbar/md$, giving the vortex collision rate as $\gamma_c = \sigma v n_v \sim (\hbar/m)n_v$. Consequently, the vortex decay rate $\gamma_v = p_a \gamma_c \propto n_v$, where p_a is the annihilation probability in the collision event. This description suggests the following rate equation for N_v ,

$$\frac{dN_v}{dt} = -\Gamma_1 N_v - \Gamma_2 N_v^2, \quad (1)$$

where the one-body decay term accounts for the drifting-out process and $\Gamma_2 = (\hbar/m)p_a/(\pi R^2)$ with $n_v = N_v/(\pi R^2)$. We find that the measured decay curves are well fit to the rate equation [Fig. 4(a)]. The numerical simulations in Ref. [26, 27] showed that the decay behavior of the vortex number becomes significantly slower at low vortex density, $n_v \xi^2 < 3 \times 10^{-3}$ ($\xi = \hbar/\sqrt{2m\mu}$ is the vortex core size), suggesting different dependence of γ_v on n_v . The vortex density in our sample is $n_v \xi^2 < 10^{-3}$

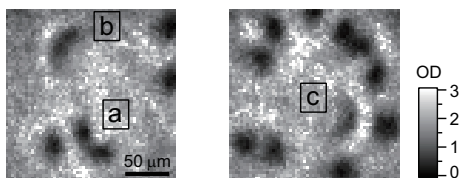


FIG. 3: Vortex pair annihilation in the turbulent superflow. Density-depleted regions with a crescent shape are observed in the condensate. These indicate coalesced vortex cores with opposite circulation. The bending structure results from the linear momentum of the vortex pair which is perpendicular to their separation direction. A tight vortex dipole (a) evolves into a dark soliton (b) with a crescent shape and eventually disappears as atoms fill up the density-depleted region (c).

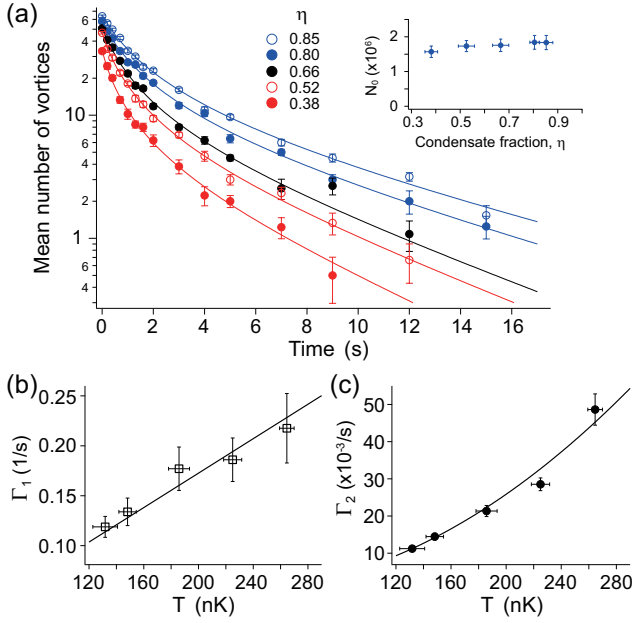


FIG. 4: (color online). Temporal evolution of the vortex number. (a) Decay curves obtained for various condensate fractions η . Each measurement consists of at least 12 realizations of the same experiment and error bars indicate the standard deviations of the mean vortex number. Solid lines are fitting curves from the rate equation in Eq (1). The inset shows the atom number of the condensate N_0 for each η . Decay rates (b) Γ_1 and (c) Γ_2 as a function of the sample temperature T . Solid lines denote linear and quadratic fitting lines to Γ_1 and Γ_2 , respectively.

and in the slow decay regime, but scrutinization of the n_v dependence of γ_v is hindered by the large one-body decay rate, $\Gamma_1 \sim 10\Gamma_2$ in our experiment. In the following, we characterize the relaxation dynamics of the turbulent condensate with the two decay rates.

We first investigate the temperature dependence of the decay rates. In order to reduce the effects from the variation of μ , which determines the vortex core size ξ as well as the condensate size R , the atom number of the condensate, $N_0 = \eta N$, is kept to be almost constant [Fig. 4(a) inset]. The total atom number N and the condensate fraction η are measured right after turning off the repulsive laser beam, and the temperature is estimated as $T = T_c(1 - \eta)^{1/3}$, where $k_B T_c = 0.94\hbar\bar{\omega}N^{1/3}$ ($\bar{\omega}$ is the geometrical mean of the trapping frequencies). The condensate fraction η was observed to decrease less than 10% even after 15 s hold time, indicating that the temperature was not varied much during the relaxation process. We note that there is built-in evaporation cooling due to the finite trap depth. The lifetime of the sample in the trap was over 60 s.

Figure 4(b) and (c) display the measured decay rates for various temperatures. Both of the decay rates monotonically increase as the temperature is increased. Remarkably, Γ_1 and Γ_2 show almost linear and quadratic

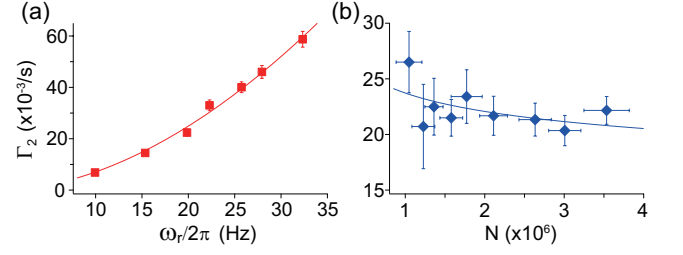


FIG. 5: (color online). Decay rate Γ_2 as a function of (a) the radial trapping frequency ω_r ($\eta \approx 0.80$ and $N \approx 2.4 \times 10^6$) and (b) the total atom number N ($\eta \approx 0.63$ and $\omega_r/2\pi = 15$ Hz). The power-law fits (solid lines) give the exponents of (a) 1.82(9) and (b) $-0.10(6)$ for ω_r and N , respectively.

dependence on the temperature, respectively, in the range of our measurement. The proportionality constants are estimated to be $C_1 = 8.6(3) \times 10^{-4} \text{ s}^{-1}\text{nK}^{-1}$ for Γ_1 and $C_2 = 6.5(4) \times 10^{-7} \text{ s}^{-1}\text{nK}^{-2}$ for Γ_2 . The one-body decay rate Γ_1 is predominantly determined from the decay behavior at low N_v and can be regarded as the damping rate of low-energy excited states of the system, in particular, with zero net vorticity. Then, the observed linear T dependence of Γ_1 seems to be comparable to the previous theoretical studies of thermal damping in nonequilibrium BEC dynamics, including low-energy excitations [28] and vortex lattice formation [29, 30].

The two-body decay rate Γ_2 , associated with the vortex pair annihilation process, reflects intricate vortex dynamics in 2D superfluid turbulence. The characteristic length scale in the vortex dynamics is given by $\xi \propto \mu^{-1/2}$. In particular, the vortex core size defines the lower bound for the vortex pair size and thus, the decay rate Γ_2 would be significantly affected by ξ . In order to investigate the μ dependence of Γ_2 , we make additional measurements of Γ_2 for various sample conditions by changing ω_r or N . To vary ω_r , we adiabatically ramp the magnetic trapping potential during the repulsive laser beam being turned off for 0.4 s.

Figure 5 shows the results of two sets of measurements for the variations of ω_r and N , respectively. In each measurement set, we controlled the condensate fraction η to be constant. The power-law fits to the data give the exponents of 1.82(9) and $-0.10(6)$ for ω_r and N , respectively. If the local two-body decay rate $(\hbar/m)p_a = (\pi R^2)\Gamma_2$ has power-law dependence on T and μ as $(\hbar/m)p_a \propto T^2\mu^\alpha$, then $\Gamma_2 \propto \omega_r^{(38+12\alpha)/15} N^{(4+6\alpha)/15}$ for a given η in the TF approximation [18]. Both of the measured exponents consistently give $\alpha = -0.9(1)$. In Fig. 6, we plot all of our Γ_2 data in the plane of $(\hbar/m)p_a$ and $(k_B T)^2/\mu$ and see that they collapse fairly well in a line. We note that the dimensionless parameter p_a is not expressed as a function of the reduced temperature T/μ , implying that the thermal relaxation in our system cannot be described in a 2D Gross-Pitaevskii model.

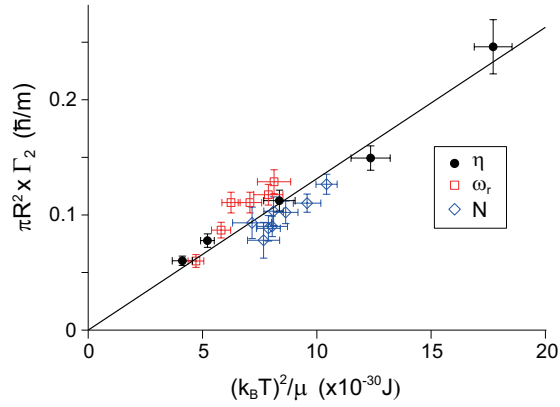


FIG. 6: (color online). Local two-body decay rate $(\pi R^2)\Gamma_2$ versus $(k_B T)^2/\mu$. R is the Thomas-Fermi radius of the condensate. The solid line denotes a linear fit to the data.

Thermal dissipation in vortex dynamics has been a central topic in quantum turbulence and addressed phenomenologically by introducing mutual frictions between quantized vortices and the normal fluid [31]. Many theoretical efforts using various approaches have been made to definitize the microscopic description of the mutual frictions in a dilute BEC system [32, 33]. However, the temperature dependence of the damping effect in the vortex motion has not been conclusively confirmed yet, for example, even for a case of a single vortex in a trapped BEC [34–37]. Our measurement results should provide a quantitative test on finite-temperature theories for vortex dynamics.

In summary, we have investigated thermal relaxation of 2D superfluid turbulence in a trapped Bose-Einstein condensate and presented clear evidence on the vortex-antivortex annihilation. One interesting extension of this work would be exploring the crossover regime from 3D to 2D by increasing the axial confinement [27, 38]. In a quasi-2D BEC with $\mu < \hbar\omega_z$, thermal phase fluctuations might qualitatively modify the relaxation behavior of quantum turbulence.

* Electronic address: yishin@snu.ac.kr

- [1] V. L. Berezinskii, Sov. Phys. JETP. **34**, 610 (1972).
- [2] J. M. Kosterlitz and D. J. Thouless, J. Phys. C **6**, 1181 (1973); J. M. Kosterlitz *ibid* **7**, 1046 (1974).
- [3] W. H. Zurek, Nature (London) **317**, 505 (1985).
- [4] S. Nazarenko, and M. Onorato, J. Low Temp. Phys. **146**, 31 (2007).
- [5] M. Tsubota, M. Kobayashi, and H. Takeuchi, Phys. Rep. **522**, 191 (2013).
- [6] T. W. Neely, E. C. Samson, A. S. Bradley, M. J. Davis, and B. P. Anderson, Phys. Rev. Lett. **104**, 160401 (2010).
- [7] D. V. Freilich, D. M. Bianchi, A. M. Kaufman, T. K. Langin, and D. S. Hall, Science **329**, 1182 (2010).
- [8] Z. Hadzibabic, P. Krüger, M. Cheneau, B. Battelier, and

- J. Dalibard, Nature (London) **441**, 1118 (2006).
- [9] J. Choi, S. W. Seo, and Y. Shin, Phys. Rev. Lett. **110**, 175302 (2013).
- [10] R. H. Kraichnan and D. Montgomery, Rep. Prog. Phys. **43**, 547 (1980).
- [11] T.-L. Horng, C.-H. Hsueh, S.-W. Su, Y.-M. Kao, and S.-C. Gou, Phys. Rev. A **80**, 023618 (2009).
- [12] R. Numasato, and M. Tsubota, J. Low Temp. Phys. **158**, 415 (2010).
- [13] R. Numasato, M. Tsubota, and V. S. L'vov, Phys. Rev. A **81**, 063630 (2010).
- [14] M. T. Reeves, B. P. Anderson, and A. S. Bradley, Phys. Rev. A **86**, 053621 (2012).
- [15] M. T. Reeves, T. P. Billam, B. P. Anderson, and A. S. Bradley, Phys. Rev. Lett. **110**, 104501 (2013).
- [16] P. M. Chesler, H. Liu, and A. Adams, Science **341**, 368 (2013).
- [17] T. W. Neely *et al.*, Phys. Rev. Lett. **111**, 235301 (2013).
- [18] In the Thomas-Fermi approximation, we estimate $\mu = (15N_0 a/\bar{a})^{2/5} \hbar\bar{\omega}/2$, where a is the scattering length of atoms, $\bar{a} = \sqrt{\hbar/m\bar{\omega}}$, and $\bar{\omega} = \omega_r^{2/3}\omega_z^{1/3}$.
- [19] S. J. Rooney, P. B. Blakie, B. P. Anderson, and A. S. Bradley, Phys. Rev. A **84**, 023637 (2011).
- [20] We turned off the magnetic potential 12 ms earlier than the optical potential. This was helpful to improve the vortex core visibility because the axial confinement direction of the optical trap was well aligned to the imaging axis [9].
- [21] See Supplemental Material for the details on the vortex counting method.
- [22] R. Onofrio *et al.*, Phys. Rev. Lett. **85**, 2228 (2000).
- [23] A. C. White, C. F. Barenghi, and N. P. Proukakis, Phys. Rev. A **86**, 013635 (2012).
- [24] E. Zaremba, T. Nikuni, and A. Griffin, J. Low Temp. Phys. **116**, 277 (1999).
- [25] S. Prabhakar, R. P. Singh, S. Gautam, and D. Angom, J. Phys. B: At. Mol. Opt. Phys. **46**, 125302 (2013).
- [26] T. Kusumura, M. Tsubota, and H. Takeuchi, J. Phys.: Conf. Ser. **400**, 012038 (2012).
- [27] J. Schole, B. Nowak, and T. Gasenzer, Phys. Rev. A **86**, 013624 (2012).
- [28] P. O. Fedichev, G. V. Shlyapnikov, and J. T. M. Walraven, Phys. Rev. Lett. **80**, 2269 (1998).
- [29] A. A. Penckwitt, R. J. Ballagh, and C. W. Gardiner, Phys. Rev. Lett. **89**, 260402 (2002).
- [30] K. Kasamatsu, M. Tsubota, and M. Ueda, Phys. Rev. A **67**, 033610 (2003).
- [31] H. E. Hall and W. F. Vinen, Proc. R. Soc. A **238**, 204 (1956).
- [32] M. Kobayashi and M. Tsubota, Phys. Rev. Lett. **97**, 145301 (2006).
- [33] N. G. Berloff and A. J. Youd, Phys. Rev. Lett. **99**, 145301 (2007).
- [34] P. O. Fedichev and G. V. Shlyapnikov, Phys. Rev. A **60**, R1779 (1999).
- [35] R. A. Duine, B. W. A. Leurs, and H. T. C. Stoof, Phys. Rev. A **69**, 053623 (2004).
- [36] B. Jackson, N. P. Proukakis, C. F. Barenghi, and E. Zaremba, Phys. Rev. A **79**, 053615 (2009).
- [37] S. J. Rooney, A. S. Bradley, and P. B. Blakie, Phys. Rev. A **81**, 023630 (2010).
- [38] J. Choi, S. W. Seo, W. J. Kwon, and Y. Shin, Phys. Rev. Lett. **109**, 125301 (2012).

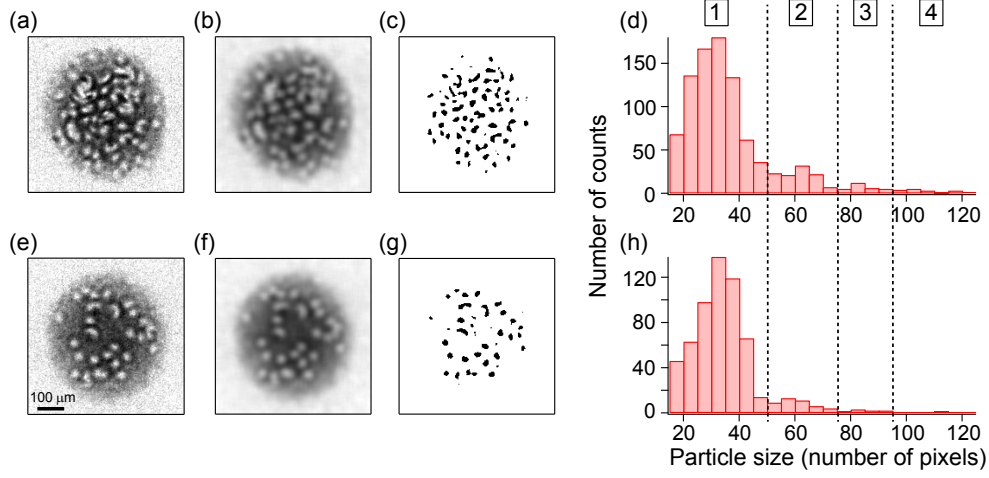


FIG. 7: Vortex number counting for a turbulent condensate with a large number of vortices. (a) Absorption image of the condensate after expansion. (b) A blurred image is obtained by applying boxcar smoothing to (a), where the box width is set to be $30 \mu\text{m}$, comparable to the vortex core size. We divide the absorption image by its blurred image and then convert it into (c) a binary image for a certain threshold value. In this image process, the density-depleted vortex cores in the absorption image are transformed into particles in the binary image. (d) Histogram of the particle size from 24 image data acquired with similar sample conditions. (e)-(h) display another example set of the image analysis, where the condensate contains about 30 vortices. The histograms show a multiple peak structure and we classify the particles by assigning a vortex number according to the particle size (dashed lines). Here, the particles having a size less than 15 are ignored. With this criterion, we determine the average total vortex number of the condensate. In comparison with hand counting, we confirmed that this method gives a consistent result within $< 10\%$. Most ambiguities in the counting come from the boundary region, but are not significant. When the total vortex number is less than 30, we counted the vortex number by hand in our data analysis.